

# Imposing neural networks and PSO optimization in the quest for optimal ankle-foot orthosis dynamic modelling

Annisa Jamali<sup>1</sup>, Aida Suriana Abdul Razak<sup>1</sup>, Shahrol Mohamaddan<sup>2</sup>

<sup>1</sup>Department of Mechanical Engineering, Faculty of Engineering, Universiti Malaysia Sarawak, Sarawak, Malaysia

<sup>2</sup>College of Engineering, Shibaura Institute of Technology, Tokyo, Japan

## Article Info

### Article history:

Received Nov 21, 2023

Revised Nov 28, 2024

Accepted Dec 26, 2024

### Keywords:

Ankle-foot orthosis

Modeling

Neural network

Particle swarm optimization

System identification

## ABSTRACT

Individuals with abnormal walking patterns due to various conditions face significant challenges in daily activities, especially walking. Ankle-foot orthosis (AFO) devices are crucial in providing essential support to their lower limbs. Accurately modeling the dynamic behavior of AFO systems, particularly in predicting ground reaction forces, is a complex yet vital task to ensure their effectiveness. This research develops dynamic models for AFO systems using advanced modeling techniques, employing both parametric and non-parametric approaches. Parametric methods, such as particle swarm optimization (PSO), and non-parametric methods, like multi-layer perceptron (MLP) neural networks, are utilized through system identification methods. According to the findings, the MLP neural network continuously generates objective results and performs exceptionally well in correctly detecting the AFO system, attaining a noticeably lower mean squared prediction error of 0.000011. This research highlights the potential of advanced modeling techniques, particularly MLP neural networks, in enhancing AFO system modeling accuracy. Although parametric techniques like PSO are useful, the MLP approach performs better, offering insightful information about modelling AFO systems and indicating that non-parametric techniques like MLP neural networks have potential to further AFO creation and control.

*This is an open access article under the [CC BY-SA](https://creativecommons.org/licenses/by-sa/4.0/) license.*



## Corresponding Author:

Annisa Jamali

Department of Mechanical Engineering, Faculty of Engineering, Universiti Malaysia Sarawak

Sarawak, Malaysia

Email: jannisa@unimas.my

## 1. INTRODUCTION

The medical condition known as a stroke happens when the brain's blood supply is interrupted, harming brain nerves and interfering with information transmission between the brain and the limbs [1]. One consequence of stroke can be foot drop, a neuromuscular disorder [2]. When walking in the swing phase, patients with foot drops drag their toes because they have difficulty dorsiflexing their feet [3]-[6].

As seen in Figure 1, these patients consequently exhibit variations from the typical gait pattern. Ankle-foot orthoses (AFOs) are frequently utilised for rehabilitation training in this situation since they offer stability and preserve range of motion. AFOs have been shown to increase gait speed when compared to non-AFO scenarios [7]-[9]. This improvement in gait velocity is important because it directly affects the quality of life for stroke survivors, allowing them to move more efficiently and reduce the risk. To ensure that patients receive the most advantages, clinicians must thus understand the mechanical properties of AFOs, such as rigidity and their effects on gait [10]-[13]. It is of the utmost importance, in clinical practice, to modify the torque of AFO in accordance with the unique body function and gait capabilities of each patient [14], [15]. Nevertheless,

conventional therapeutic approaches that rely on manual support are laborious for practitioners and could not offer continuous assistance for prolonged durations [16], [17].

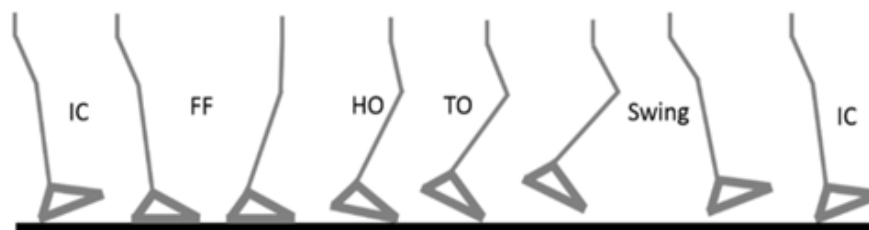


Figure 1. Walking gait phase; initial contact (IC), foot flat (FF), heel-off (HO), and toe-off (TO) [12]

Modeling AFO is challenging, particularly when considering ground reaction forces in complex systems with multiple points of ground contact [18]. AFO models have been created using a variety of techniques, such as musculoskeletal simulations, direct multiple shooting techniques, Monte Carlo simulations, computational modelling and functional electrical stimulations [19], [20]. In recent years, system identification has gained attention for accurately modeling dynamic systems. Parametric identification involves two phases: qualitative operation, which establishes the system's structure, and identification, which determines numerical values for structural parameters. Traditional methods like the least squares method and Zatsiorsky regression equations have been used for parametric identification [21]. The goal is to apply this control method's inverse dynamic model to human gait systems.

While genetic algorithms are well-known as a stochastically optimal approach, particle swarm optimization (PSO), another global optimization algorithm, has gained prominence [22]. PSO relies on social information exchange among members of a group to find specific parameter sets that optimize an objective function. It is suitable for nonlinear design spaces with discontinuities and diverse constraints.

Non-parametric models often incorporate components of soft computing methods, such as neural networks (NNs) and fuzzy logic. Deep neural networks consist of layers of artificial neurons that mimic biological neurons' functioning, making them effective for various machine learning tasks. Decision trees, utilized in random forests, contribute to the final classification by aggregating judgments based on input variables. Research indicates that deep neural network models perform well, particularly in predicting the need for AFOs [23].

The aim of this research is to explore the performance of the dynamic model for AFO using parametric and non-parametric modelling methodologies. The parametric approach involves the utilization of PSO, while the non-parametric approach employs multi-layer perceptron (MLP) neural networks. These models are created using information obtained from an experimental setup and the system identification approach. Following model development, a thorough validation process ensues, with the acquired results subject to meticulous comparison and analysis. The findings provide to improving the development and control of AFO systems, benefiting individuals with mobility impairments caused by conditions like foot drop, stroke, and other disabilities.

## 2. METHOD

This study presents a comprehensive approach to modeling an AFO, as illustrated in Figure 2. The proposed algorithm is designed to accurately replicate the dynamic behavior of the ankle. By incorporating both parametric and non-parametric techniques, the study explores various modeling options to identify the most effective approach. Ultimately, this modeling framework aims to enhance the development and control of AFOs, ensuring they closely mimic the natural dynamics of the ankle.

### 2.1. Experimentation set up and data acquisition

Initially, an AFO rig with one degree of freedom (DOF) was designed and fabricated. The structure specifically designed for children utilized 3D printing materials, boasting approximate dimensions of  $0.15 \text{ m} \times 0.05 \text{ m} \times 0.03 \text{ m}$ . Table 1 outlines the specifications of the instrumentation employed in this study.

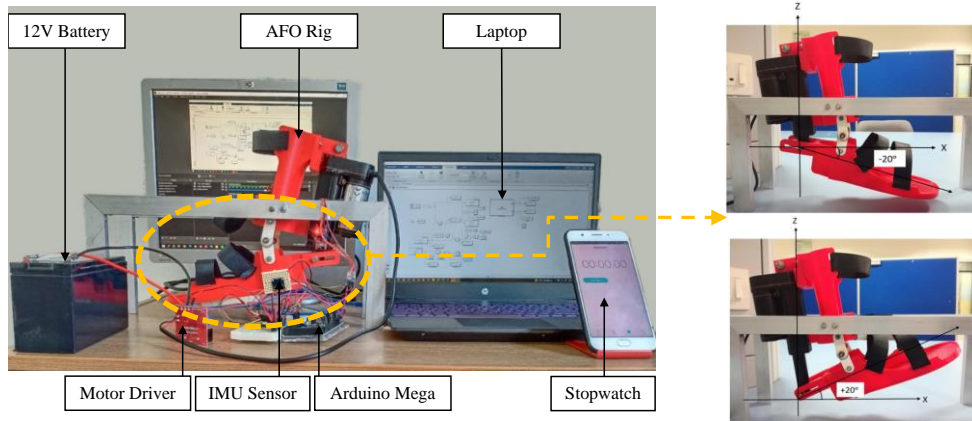


Figure 2. The experimental setup of AFO

Table 1. The AFO instrumentation

Item	Specification
Model size (L×W×H)	0:15 m 0:05 m 0:03 m
Motor	Linear actuator: 12 V, 51 mm stroke and 900 N load rating
Motor driver	L298N: 2 A, 5-35 V
Power supply	12 V
Sensor	IMU sensor: MPU 6050
Microcontroller	Arduino Mega

The primary objective of this setup was to capture the input-output dynamics of the AFO during rehabilitation sessions, specifically focusing on dorsiflexion and plantarflexion movements. To facilitate mobility, a linear actuator exerted force onto the AFO at the rear of the foot brace, thereby transferring kinetic energy, as depicted in Figure 2. A linear actuator was specifically chosen because of its long-term dependability, high torque capacity, and accurate stroke control.

The linear actuator was interfaced with a motor driver (L298N), which in turn was controlled by the Arduino Mega microcontroller. This microcontroller was connected to a computer via USB connection. The configuration of the rig allowed for a dorsiflexion angle of +20 degrees and a plantarflexion angle of -20 degrees. IMU sensor was utilized to detect the angular movement during exercises, specifically representing feet dorsiflexion and plantarflexion, as depicted in the schematic diagram of Figure 3. This sensor was directly linked to the data acquisition system, comprising the Arduino Mega microcontroller, which, in turn, connected to a computer via USB.

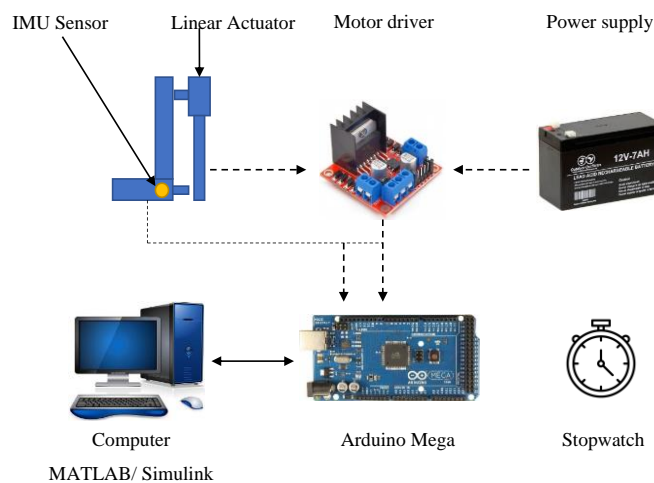


Figure 3. Schematic diagram of AFO

A personal notebook with a powerful processor, 4.00 GB of RAM, and MATLAB software was used to analyse the generated signals. The Simulink program was used to create the interface for data gathering. An other technique was to apply a bang-bang torque signal to the AFO in order to simultaneously activate the actuator with the required torque.

## 2.2. System identification

The dynamic system of the AFO was modelled in this work using the system identification technique. In this technique, four main stages were involved that is data acquisition, model structure selection, model estimation, and model validation. To explore the effects of parametric and non-parametric approaches, the model estimation in this study was conducted using PSO and MLPNN, respectively. Subsequently, system identifications were formulated utilizing an auto-regressive with exogenous (ARX) and nonlinear auto-regressive with exogenous (NARX) model structure, correspondingly. The ARX model structure is describe in (1):

$$y(t) = \frac{B(z^{-1})}{A(z^{-1})}u(t) + \frac{\varepsilon(t)}{A(z^{-1})} \quad (1)$$

where the expressions of  $A(z^{-1})$  and  $B(z^{-1})$  are;

$$\begin{aligned} A(z^{-1}) &= 1 + a_1z^{-1} + \dots + a_nz^{-n} \\ B(z^{-1}) &= b_0 + b_1z^{-1} + \dots + b_nz^{-(n-1)} \end{aligned} \quad (2)$$

White noise,  $\varepsilon(t)=0$ ,  $n$  is the model's orders, and  $[a_1, \dots, a_n, b_1, \dots, b_n]$  are the model parameters that need to be estimated to determine  $z^{-1}$ . The system's output vector is denoted by  $y(t)$  and its input vector by  $u(t)$ . In (3) yields the neural network auto regressive model with eXogenous inputs (NNARX) model structure regression vector. Through the integration of neural networks into the model framework, NNARX overcomes the drawbacks of NARX.

$$\varphi(t) = [y(t-1), \dots, y(t-n_a), u(t-k), \dots, u(t-n_b-n_k+1)]^T \quad (3)$$

where  $\varphi(t)$  denotes the regression vector at time step,  $t$ . Past values of the system's input and output are used to generate the regression vector. In (4) gives the one step ahead (OSA) forecast of the NNARX model:

$$\hat{y}\left(\frac{t}{\theta}\right) = y\left(\frac{t}{t-1}, \theta\right) = g(\varphi(t), \theta) \quad (4)$$

where  $g$  is the function that the neural network approach has achieved.

### 2.2.1. Parametric estimation via particle swarm optimization

Parametric system identification involves utilizing measurable data to develop mathematical models that represent a dynamic system [24]. Good models are necessary for most model-based control methods. The key task after defining the model structure is to estimate its parameters, typically determined by applying a global minimum criterion function. PSO was inspired by the study of natural social behaviors in animals, such as schools of fish, swarms of bees, and bird flocks, and operates based on a population model [25]. PSO is easy to apply to a variety of optimisation issues and has a straightforward approach. Although it can be challenging to initialise its parameters. Despite the fact that initialising its parameters can be difficult, PSO has a high chance and efficiency of finding the global optima and requires few modifications. PSO can converge too quickly and get stuck in local optima, despite its quick error convergence.

In the process of identifying the optimal solution in multidimensional space, the PSO algorithm mimics birds using  $N$  particles [26]. Position ( $P_i$ ) and velocity ( $V_i$ ), where  $i$  is the particle label, are the two characteristics of every particle. The particle's movement is represented by ( $V_i$ ), as seen in (5). ( $P_i$ ) is the outcome of the particle's motion and a potential solution to the associated optimisation problem, as illustrated in (6). Each particle's fitness value  $F_i$ , which is calculated using mean squared error (MSE), quantifies the difference between the current candidate solution and the best solution. The individual extremum  $G_i$  is the optimal solution for individual particle search, in contrast to its historical and present solutions. For the whole particle swarm, the population extremum  $Z$  is the best solution relative to its historical solution and all individual extremum of the current generation. The particle population continuously updates the position and velocity of particles by monitoring both individual and group extremums during the search and iteration process in order to identify the optimal solution that satisfies the requirements. The optimisation outcome can be seen in the final group extremum  $Z$ .

$$V_{i-new} = \omega V_i + c_1 rand()(G_i - P_i) + c_2 rand()(Z - P_i) \quad (5)$$

$$V_{i-new} = V_i + P_i \quad (6)$$

where the left part of the equation represents the new velocity and position of the particle in the current generation, and the right part represents the particle properties from the previous generation. The inertia factor  $\omega$  is equal to 0.5.  $c_1$  and  $c_2$  are learning factors with values of 2. In addition, the population size  $N$  (1,599) was adjusted to  $N/2$ , resulting in 799.5 and the maximum number of iterations  $M$  was set to 1,000.

### 2.2.2. Non-parametric estimation by using multi-layer perceptron neural network

The AFO was modelled using an MLP neural network for non-parametric estimation. The MLP neural network family is the most commonly utilised because it can estimate a very complex formula association while producing a simple model [27]. In the MLP, the input layer is formed by a single set of nodes, and the output is generated by a second layer, with several hidden layers positioned between them. The input layer  $x_i$ , output layer  $y_j$ , and hidden layer  $w_{ij}$  with different strength weights make up the network layer. The qualities of the function  $f(\cdot)$  include radial basis, hyperbolic tangent, sigmoid, threshold, and linear. The network can forecast the output,  $\hat{y}$ , as precisely as feasible thanks to the mapping. In (7), the MLP output is displayed:

$$\hat{y}(w, W) = F_i(\sum_{j=1}^q W_{ij} \cdot f_j(\sum_{i=1}^m w_{ij} X_i + w_{j0}) + W_{i0}) \quad (7)$$

Levenberg-Marquardt (LM) is chosen for training networks because of its fast convergence, even though it demands higher memory usage compared to alternative algorithms. The LM minimises the residual,  $\varepsilon(t, \theta) = y(t) - \hat{y}(t, \theta)$ , in order to maximise the error based on the criterion in (8):

$$L^i(\theta) = \left(\frac{1}{2N}\right) \sum_{t=1}^N \varepsilon^{-2}(t, \theta) \approx P_N(\theta, Z^N) \quad (8)$$

where  $Z^N$  represents the training data set.

### 2.2.3. Model validation

To ensure the adequacy of the model under development, the validation phase is essential [15]. This validation process employs three methods: OSA prediction, MSE, and correlation test. The study examines five correlation functions:

$$\begin{aligned} \varphi_{\varepsilon\varepsilon}(\tau) &= E[\varepsilon(t - \tau)\varepsilon(t)] = \delta(\tau), \\ \varphi_{u\varepsilon}(\tau) &= E[u(t - \tau)\varepsilon(t)] = 0, \forall \tau, \\ \varphi_{\varepsilon^2\varepsilon}(\tau) &= E[u^2(t - \tau) - \bar{u}^2(t)\varepsilon(t)] = 0, \forall \tau, \\ \varphi_{\varepsilon^2\varepsilon^2}(\tau) &= E[u^2(t - \tau) - \bar{u}^2(t)\varepsilon^2(t)] = 0, \forall \tau, \\ \varphi_{\varepsilon(\varepsilon u)}(\tau) &= E[\varepsilon(t)\varepsilon(t - 1 - \tau)u(t - 1 - \tau)] = 0, \tau \geq 0, \end{aligned} \quad (9)$$

$\varepsilon u(t) = \varepsilon(t + 1)u(t + 1)$ ,  $\delta(\tau)$  is an impulse function, and  $\varphi_{u\varepsilon}(\tau)$  is the cross-correlation function between  $u(t)$  and  $\varepsilon(t)$ . All five requirements need to be met because the MLP model is built using the NARX structure, which makes it a nonlinear system. Conversely, another PSO model employing a linear system necessitates the fulfillment of only three conditions.

The study employs 1,599 data points for PSO and 2,189 data points for MLP in testing. The selection of 1,599 data points for PSO aims for increased stability in results, while 2,189 data points for MLP correspond to the entirety of five walking cycles during the experiment. The 95% confidence bands are used, which are around  $\pm 1.96/\sqrt{N}$  ( $N$  data), with one or more function points falling outside of these limits indicating a substantial link [28]. The model is deemed adequate if the correlation functions remain within the confidence intervals.

## 3. RESULTS AND DISCUSSION

In this research, the collected datasets were split into two parts: one for training the model and the other for evaluating its performance. The validation of the developed system involved multiple metrics, including MSE, OSA prediction, correlation tests, and examination of the pole-zero diagram for stability.

The most appropriate model was chosen primarily based on robustness studies, with an emphasis on achieving a low MSE, high stability, and unbiased outcomes in correlation tests. These evaluations were critical

to ensuring that the developed model performed very well. Since there was no prior understanding of the optimal model for an AFO, the structure realization process employed a heuristic method.

### 3.1. Modelling using particle swarm optimization

The dataset utilized for parametric modeling with PSO comprised 1,599 data points, which were divided into two equal sets of 799.5 data points each. The second set served as the validation test set, and the first set served as the modelling estimation set. MSE, stability criteria and two correlation tests were used to evaluate the transfer function in the PSO modelling process in order to validate the findings. It was determined that a model order of four yielded the most favorable outcomes. The PSO algorithm was configured with a maximum of 1000 iterations and a swarm size of 400.

Figure 4 illustrates the PSO predictions of the roll axis angle. The graph demonstrates that PSO managed to approximate certain aspects of the actual data. However, noticeable disparities exist between the actual and predicted PSO outputs. Further investigation on Figure 5 about correlation tests for each roll axis angle show that all fall outside of its 95% confidence interval. This signifies that there is bias in the model.

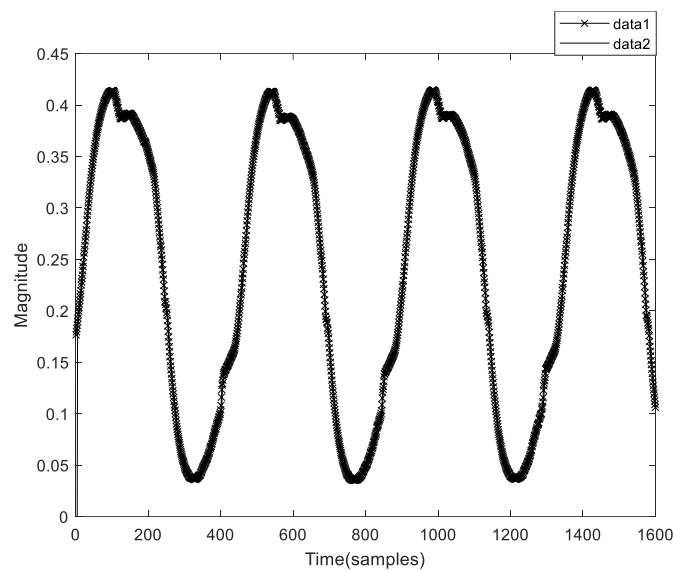


Figure 4. The output and estimated output of roll axis angle

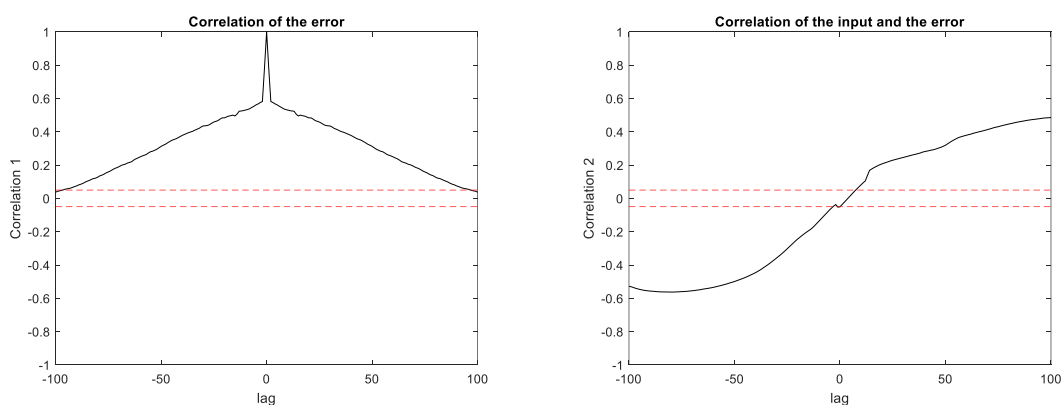


Figure 5. The correlation test for roll axis angle (PSO)

Figure 6 shows the stability test result, which shows that the poles are visible inside the unity circle and the zeros are at the origin. For “×,” the poles represent the symbol, while for “○,” the zero. Due to the poles’ placement inside the unit circle, the system is stable.

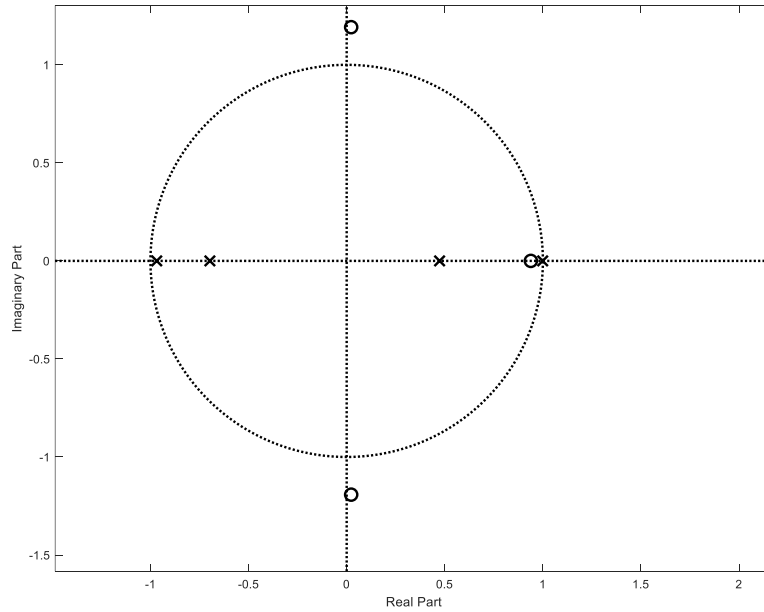


Figure 6. The stability test for roll axis angle (PSO)

Table 2 presents the numerical outcomes of the optimal model order. It is noteworthy that each model demonstrates bias, prompting the utilization of MSE values as indicators for determining the superior model. Among the various model orders evaluated, it was found that model order 4 yielded the lowest MSE values for both the training and testing datasets, which were  $1.8075 \times 10^{-4}$  and  $1.7743 \times 10^{-5}$ , respectively, thus establishing it as the optimal model for PSO optimization method.

Table 2. Comparison of PSO optimization performance in different number of model order

Model order	MSE in training data	MSE in testing data	Stability	Correlation test
2	$1.3612 \times 10^{-4}$	$6.1793 \times 10^{-5}$	Unstable	Biased
4	$1.8075 \times 10^{-4}$	$1.7743 \times 10^{-5}$	Stable	Biased
6	$2.6758 \times 10^{-4}$	$1.2621 \times 10^{-5}$	Stable	Biased
8	$4.4309 \times 10^{-4}$	$8.9236 \times 10^{-5}$	Unstable	Biased
10	$9.7826 \times 10^{-4}$	$5.2718 \times 10^{-4}$	Unstable	Biased

### 3.2. Modelling using multi-layer perceptron

The dataset comprising 2,189 data points for non-parametric modeling with neural network multi-layer perceptron (NN MLP) was split into two sets: one containing 1,532 points for modeling (the estimation set) and the other containing 657 points for validation (the test set). To validate the results, the NN MLP modeling was compared using MSE and five correlation tests. Given the lack of prior knowledge regarding appropriate delay numbers and model structures for NN MLP, a heuristic method was employed to determine the structure.

During this technique, three crucial factors were considered: the error, the size of the NN structure (or the number of neurones), and the number of delay signals. Due to the randomness involved in selecting the best model, assessing the final component was crucial in determining the ideal number of delay signals and the configuration for each model. Validation MSE, modelling MSE, and correlation tests were used to determine the selection criteria.

The study started with a model structure of [2 2 1], which included one neurone in the output layer, two neurones in the second hidden layer, and two neurones in the first hidden layer. The delay number served as a representation of the input layer. Eight delay signals, eight neurones in the first and second hidden layers, and one neurone in the output layer were then used to improve model performance, resulting in a model structure of [8 8 1]. Figure 7 shows the MLP predictions for the roll axis angle, with the actual data shown by a vertical line at point 1,532. With a nearly zero difference between the real and anticipated MLP output, the graph shows how well the MLP tracks the actual data.

Figure 8 shows the correlation test results for all roll axis angles. The accurateness of the model is demonstrated by the MLP results, which clearly lie inside the 95% confidence level. This underscores the unbiased nature of the model's predictions. Table 3 displays the numerical results pertaining to the optimal model structure and delay of NN MLP. Among the listed configurations, the model structure [8 8 1] with 8 delays stands out, showcasing the lowest MSE of  $1.1034 \times 10^{-5}$ , thus confirming its status as the best-performing model.

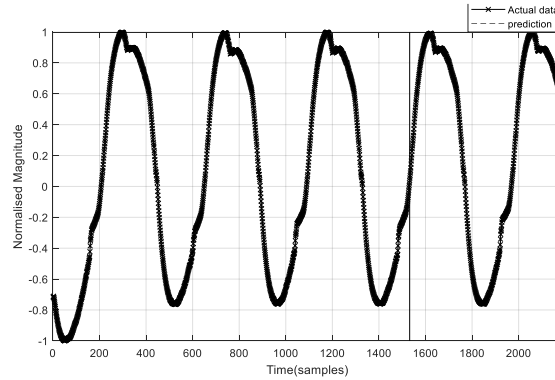


Figure 7. The output and estimated output of roll axis angle (MLP)

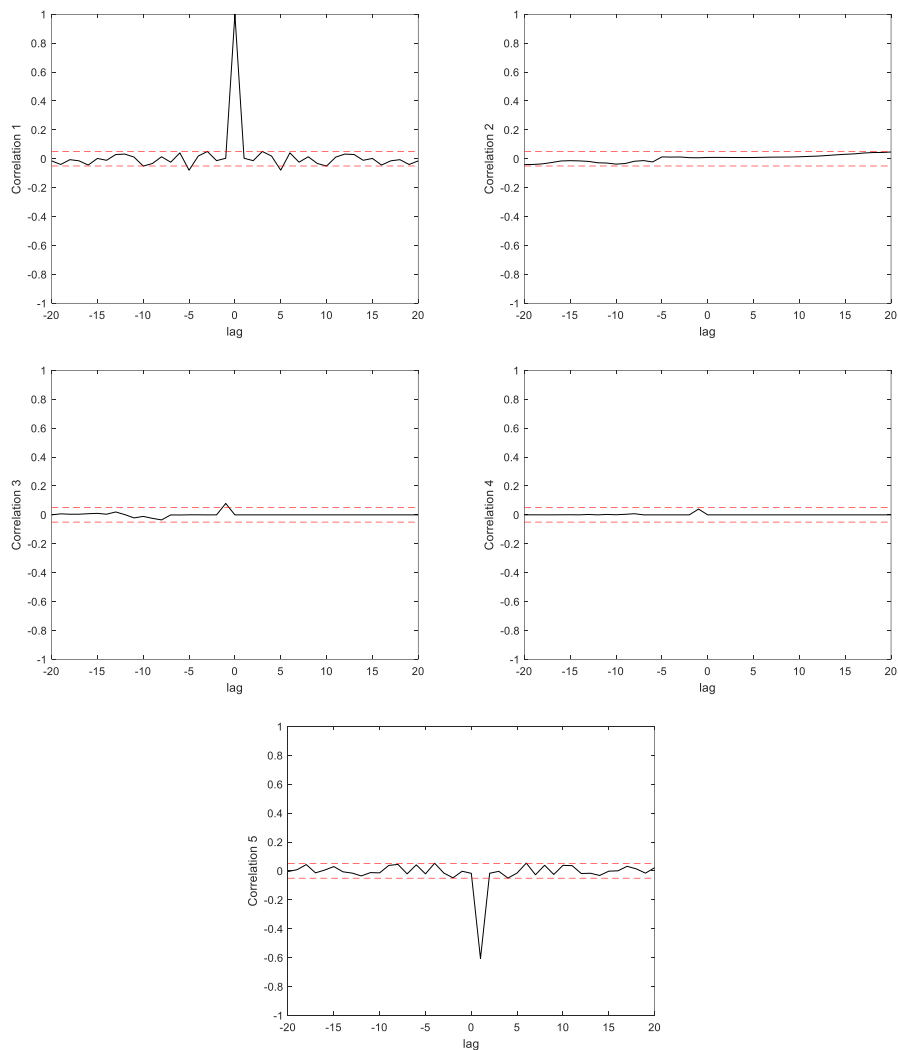


Figure 8. The correlation test for roll axis angle (MLP)



Table 3. Comparison of NN MLP performance

Model structure	Delay	MSE	Correlation test
[2 2 1]	2	$2.3829 \times 10^{-4}$	Unbiased
[4 4 1]	2	$3.5671 \times 10^{-4}$	Unbiased
[6 6 1]	6	$2.7149 \times 10^{-4}$	Unbiased
[8 8 1]	7	$1.8625 \times 10^{-4}$	Unbiased
[8 8 1]	8	$1.1034 \times 10^{-5}$	Unbiased

### 3.3. Comparative assessment and discussion

Thorough training and testing protocols, together with extensive correlation studies, have been used to validate PSO and NN MLP-based models. The outcomes of these assessments consistently show that the different modelling approaches taken into consideration in this study function satisfactorily. With an emphasis on mean-squared error and correlation test results, Table 3 provides a succinct overview of the relative effectiveness of parametric and non-parametric modelling techniques.

When comparing the performance of the two modelling methodologies, Table 4 demonstrates that the NN MLP-based non-parametric approach offers a better approximation to the system response than PSO. This conclusion is consistent with earlier studies showing that parametric modelling techniques like GA typically produce inferior results versus non-parametric techniques like NN MLP [13]. Additionally, the results of the correlation test show that NN MLP performs better than PSO, showing a smaller mean-squared error.

Table 4. Performance of parametric and non-parametric modelling approaches

Algorithm	MSE	Correlation test
NN MLP	0.000011034	Unbiased
PSO	0.00018075	Biased

However, a notable advantage of PSO lies in its fewer parameters requiring tuning. Despite its capability to find the best solution through particle interaction, as dictated by (5), PSO progresses relatively slowly toward the global optimum due to the high-dimensional search space [29]. Moreover, it tends to generate suboptimal outcomes when confronted with complex and extensive datasets.

These results highlight the effectiveness of using NN MLP to address difficult nonlinear problems while managing substantial amounts of input data. NN MLP is a practical tool for both researchers and practitioners across a range of fields because it generates predictions quickly after training. Remarkably, even with smaller sample sizes, NN MLP maintains a comparable accuracy ratio, highlighting its robustness and versatility.

## 4. CONCLUSION

The modelling of an AFO using both PSO and NN MLP has been detailed, encompassing parametric and non-parametric techniques. The AFO moves along the x-axis through bang-bang torque application, with motion data collected via Simulink and ankle angle measured using an IMU sensor, processed by an Arduino Mega. The modelling occurs within the MATLAB/Simulink environment and is validated through training, test validation, mean-squared error analysis, and correlation tests. Findings indicate that NN MLP outperforms PSO in modelling AFO. The most effective NN MLP model will be applied in developing control strategies to regulate the AFO ankle angle, examining control schemes to address varying constraints or disturbances before the experimental phase. Future studies could concentrate on enhancing these models' precision and resilience to various environmental factors and disturbances. The responsiveness and performance of AFO systems may also be improved by looking at the integration of real-time adaptive control methods with NN MLP models. Investigating other advanced machine learning techniques and hybrid approaches may provide valuable insights and improvements. Finally, conducting extensive clinical trials will be essential to validate these models and control strategies in real-world scenarios, ensuring their practical efficacy and reliability.





## ACKNOWLEDGEMENTS

The authors would like to express their gratitude to the Minister of Higher Education Malaysia (MOHE) and Universiti Malaysia Sarawak (UNIMAS) for funding and providing facilities to conduct this study.

## REFERENCES

- [1] A. M. Joshua, Z. Misri, S. Rai, and V. H. Nampoothiri, "Stroke," in *Physiotherapy for Adult Neurological Conditions*, Singapore: Springer Nature Singapore, 2022, pp. 185–307, doi: 10.1007/978-981-19-0209-3\_3.
- [2] M. Vali, V. Petrović, S. Boersma, J. W. van Wingerden, L. Y. Pao, and M. Kühn, "Adjoint-based model predictive control for optimal energy extraction in waked wind farms," *Control Engineering Practice*, vol. 84, pp. 48–62, Mar. 2019, doi: 10.1016/j.conengprac.2018.11.005.
- [3] S. Prenton, K. L. Hollands, and L. P. J. Kenney, "Functional electrical stimulation versus ankle foot orthoses for foot-drop: A meta-analysis of orthotic effects," *Journal of Rehabilitation Medicine*, vol. 48, no. 8, pp. 646–656, 2016, doi: 10.2340/16501977-2136.
- [4] C. Peishun, Z. Haiwang, L. Taotao, G. Hongli, M. Yu, and Z. Wanrong, "Changes in Gait Characteristics of Stroke Patients with Foot Drop after the Combination Treatment of Foot Drop Stimulator and Moving Treadmill Training," *Neural Plasticity*, pp. 1–5, Nov. 2021, doi: 10.1155/2021/9480957.
- [5] N. Shah and K. Vemulapalli, "Foot Drop Secondary to Ankle Sprain in Two Paediatric Patients: A Case Series," *Cureus*, Jun. 2022, doi: 10.7759/cureus.26398.
- [6] O. Eldirdiry, R. Zaier, A. Al-Yahmedy, I. Bahadur, and F. Alnajjar, "Modeling of a biped robot for investigating foot drop using MATLAB/Simulink," *Simulation Modelling Practice and Theory*, Oct. 2020, doi: 10.1016/j.simpat.2020.102072.
- [7] H. M. Nazha, S. Szávai, M. A. Darwich, and D. Juhre, "Passive Articulated and Non-Articulated Ankle-Foot Orthoses for Gait Rehabilitation: A Narrative Review," *Healthcare (Switzerland)*, vol. 11, no. 7, pp. 1–18, Mar. 2023, doi: 10.3390/healthcare11070947.
- [8] J. Laidler, "The impact of ankle-foot orthoses on balance in older adults: A scoping review," *Canadian Prosthetics and Orthotics Journal*, vol. 4, no. 1, Jan. 2021, doi: 10.33137/cpoj.v4i1.35132.
- [9] P. Fonseca *et al.*, "Does gait with an ankle foot orthosis improve or compromise minimum foot clearance?," *Sensors*, vol. 21, no. 23, pp. 1–9, Dec. 2021, doi: 10.3390/s21238089.
- [10] T. Kobayashi, F. Gao, N. Lecursi, K. B. Foreman, and M. S. Orendurff, "Effect of shoes on stiffness and energy efficiency of ankle-foot orthosis: Bench testing analysis," *Journal of Applied Biomechanics*, vol. 33, no. 6, pp. 460–463, 2017, doi: 10.1123/jab.2016-0309.
- [11] M. Yamamoto, K. Shimatani, H. Okano, and H. Takemura, "Effect of Ankle-Foot Orthosis Stiffness on Muscle Force during Gait through Mechanical Testing and Gait Simulation," *IEEE Access*, vol. 9, pp. 98039–98047, 2021, doi: 10.1109/ACCESS.2021.3095530.
- [12] S. Ramezani, B. Brady, H. Kim, M. K. Carroll, and H. Choi, "A Method for Quantifying Stiffness of Ankle-Foot Orthoses Through Motion Capture and Optimization Algorithm," *IEEE Access*, vol. 10, pp. 58930–58937, 2022, doi: 10.1109/ACCESS.2022.3178701.
- [13] A. Coccia *et al.*, "Biomechanical modelling for quantitative assessment of gait kinematics in drop foot patients with ankle foot orthosis," in *2022 IEEE International Symposium on Medical Measurements and Applications, MeMeA 2022 - Conference Proceedings*, IEEE, Jun. 2022, pp. 1–6, doi: 10.1109/MeMeA54994.2022.9856549.
- [14] C. Zhou, Z. Yang, K. Li, and X. Ye, "Research and Development of Ankle-Foot Orthoses: A Review," *Sensors*, vol. 22, no. 17, pp. 1–15, Sep. 2022, doi: 10.3390/s22176596.
- [15] W. Wu, H. Zhou, Y. Guo, Y. Wu, and J. Guo, "Peg-in-hole assembly in live-line maintenance based on generative mapping and searching network," *Robotics and Autonomous Systems*, vol. 143, pp. 1–11, Sep. 2021, doi: 10.1016/j.robot.2021.103797.
- [16] M. Hamedani, V. Prada, P. Tognetti, V. Leoni, and A. Schenone, "Robot-assisted and traditional intensive rehabilitation therapy in the treatment of post-acute stroke patient: the experience of a standard rehabilitation ward," *Neurological Sciences*, vol. 43, no. 6, pp. 3999–4001, Jun. 2022, doi: 10.1007/s10072-022-06041-8.
- [17] S. Fatone, W. B. Johnson, and K. Tucker, "A three-dimensional model to assess the effect of ankle joint axis misalignments in ankle-foot orthoses," *Prosthetics and Orthotics International*, vol. 40, no. 2, pp. 240–246, 2016, doi: 10.1177/0309364613516488.
- [18] M. Sreenivasa, M. Millard, M. Felis, K. Mombaur, and S. I. Wolf, "Optimal control based stiffness identification of an ankle-foot orthosis using a predictive walking model," *Frontiers in Computational Neuroscience*, vol. 11, Apr. 2017, doi: 10.3389/fncom.2017.00023.
- [19] M. Rosenberg and K. M. Steele, "Simulated impacts of ankle foot orthoses on muscle demand and recruitment in typically developing children and children with cerebral palsy and crouch gait," *PLoS ONE*, vol. 12, no. 7, 2017, doi: 10.1371/journal.pone.0180219.
- [20] A. K. Hegarty, A. J. Petrella, M. J. Kurz, and A. K. Silverman, "Evaluating the effects of ankle-foot orthosis mechanical property assumptions on gait simulation muscle force results," *Journal of Biomechanical Engineering*, vol. 139, no. 3, 2017, doi: 10.1115/1.4035472.
- [21] J. T. Bryson, X. Jin, and S. K. Agrawal, "Optimal design of cable-driven manipulators using particle swarm optimization," *Journal of Mechanisms and Robotics*, vol. 8, no. 4, 2016, doi: 10.1115/1.4032103.
- [22] Y. J. Choo, J. K. Kim, J. H. Kim, M. C. Chang, and D. Park, "Machine learning analysis to predict the need for ankle foot orthosis in patients with stroke," *Scientific Reports*, vol. 11, no. 1, 2021, doi: 10.1038/s41598-021-87826-3.
- [23] D. Adiputra *et al.*, "A review on the control of the mechanical properties of Ankle Foot Orthosis for gait assistance," *Actuators*, vol. 8, no. 1, 2019, doi: 10.3390/act8010010.
- [24] I. Z. M. Darus and M. O. Tokhi, "Parametric and non-parametric identification of a two dimensional flexible structure," *Journal of Low Frequency Noise Vibration and Active Control*, vol. 25, no. 2, pp. 119–143, 2006, doi: 10.1260/026309206778494274.
- [25] M. S. Amiri, R. Ramli, M. F. Ibrahim, D. A. Wahab, and N. Aliman, "Adaptive particle swarm optimization of pid gain tuning for lower-limb human exoskeleton in virtual environment," *Mathematics*, vol. 8, no. 11, pp. 1–16, 2020, doi: 10.3390/math8112040.
- [26] D. Jin, Y. Liu, X. Ma, and Q. Song, "Long time prediction of human lower limb movement based on IPSO-BPNN," *Journal of Physics: Conference Series*, 2021, vol. 1865, no. 4, doi: 10.1088/1742-6596/1865/4/042099.
- [27] A. Jamali, I. Z. M. M. Darus, P. M. Samin, and M. O. Tokhi, "Intelligent modeling of double link flexible robotic manipulator using artificial neural network," *Journal of Vibroengineering*, vol. 20, no. 2, pp. 1021–1034, 2018, doi: 10.21595/jve.2017.18575.
- [28] G. Casella and R. L. Berger, *Statistical Inference*, 2nd ed. Pacific Grove, CA, USA: Duxbury, 2002.
- [29] A. G. Gad, "Particle Swarm Optimization Algorithm and Its Applications: A Systematic Review," *Archives of Computational Methods in Engineering*, vol. 29, no. 5, pp. 2531–2561, 2022, doi: 10.1007/s11831-021-09694-4.





**BIOGRAPHIES OF AUTHORS**

**Annisa Jamali**     received her B.E. (2006) and M.E. (2011) degrees in Mechatronics Engineering from International Islamic University Malaysia and later her Ph.D. in Mechanical Engineering from Universiti Teknologi Malaysia (UTM). Currently, she is a Senior Lecturer at Faculty of Engineering, Universiti Malaysia Sarawak (UNIMAS). Her current research interests include robotics and automation, modelling and simulation of dynamic systems and artificial intelligent techniques for system identification and control. She can be contacted at email: jannisa@unimas.my.



**Aida Suriana Abdul Razak**     received her B.E. (2019) in Mechanical and Manufacturing Engineering from Universiti Malaysia Sarawak (UNIMAS). Currently, she is a Postgraduate Student at Faculty of Engineering, Universiti Malaysia Sarawak (UNIMAS). She can be contacted at email: aida.suriana@gmail.com.



**Shahrol Mohamaddan**     is an Associate Professor at the College of Engineering, Shibaura Institute of Technology (SIT), Japan. He graduated with Bachelor and Master of Engineering (Mechanical) from SIT, Japan and completed his Ph.D. in Ergonomics from Loughborough University, UK. With over 15 years of research experience, he has authored more than 100 publications spanning engineering, robotics, and biomedical applications. His recent work focuses on upper limb rehabilitation devices and human musculoskeletal modeling. Currently, he is the head of Ergonomics and Biomechanics Laboratory at the SIT. He can be contacted at email: mshahrol@shibaura-it.ac.jp.